Supplement of Atmos. Chem. Phys., 19, 8547–8562, 2019
https://doi.org/10.5194/acp-19-8547-2019-supplement

Atmospheric Chemistry and Physics
Open Access
EGU

Supplement of

An improved estimate for the δ^{13}C and δ^{18}O signatures of carbon monoxide produced from atmospheric oxidation of volatile organic compounds

Isaac J. Vimont et al.

Correspondence to: Isaac J. Vimont (isaac.vimont@colorado.edu)

Authors:

*Isaac J Vimont[1,2,3], Jocelyn C. Turnbull[3,4], Vasilii V. Petrenko[5], Philip F. Place[5], Colm Sweeney[2], Natasha Miles[6], Scott Richardson[6], Bruce H. Vaughn[1], James W.C. White[1]

1. Institute of Arctic and Alpine Research, Boulder, CO USA
2. National Oceanic and Atmospheric Administration, Global Monitoring Division, Boulder, CO USA
3. CIRES, University of Colorado, Boulder, CO, USA
4. GNS Science, Lower Hutt, New Zealand
5. University of Rochester Earth and Environmental Science Department, Rochester, NY, USA
6. Pennsylvania State University, College Station, PA USA

* Corresponding Author: Isaac.vimont@colorado.edu

S.1 Broadleaf, Deciduous vegetation cover at Indianapolis and Beech Island

Using the MEGAN 2.1 model plant functional type (PFT) inputs (Guenther et al., 2012), we created land cover maps for Indianapolis (figure S1) and Beech Island (Figure S2). These plants produce the bulk of biogenic VOC emissions (e.g. Harley et al., 1999) and therefore these plants are most relevant to our study.

Figure S1: Broadleaf, deciduous trees and shrubs for the region surrounding Indianapolis, IN. The black circle denotes the location of Indinapolis and its immediate surroundings. The grid is incremented at 0.5° (both latitude and longitude).

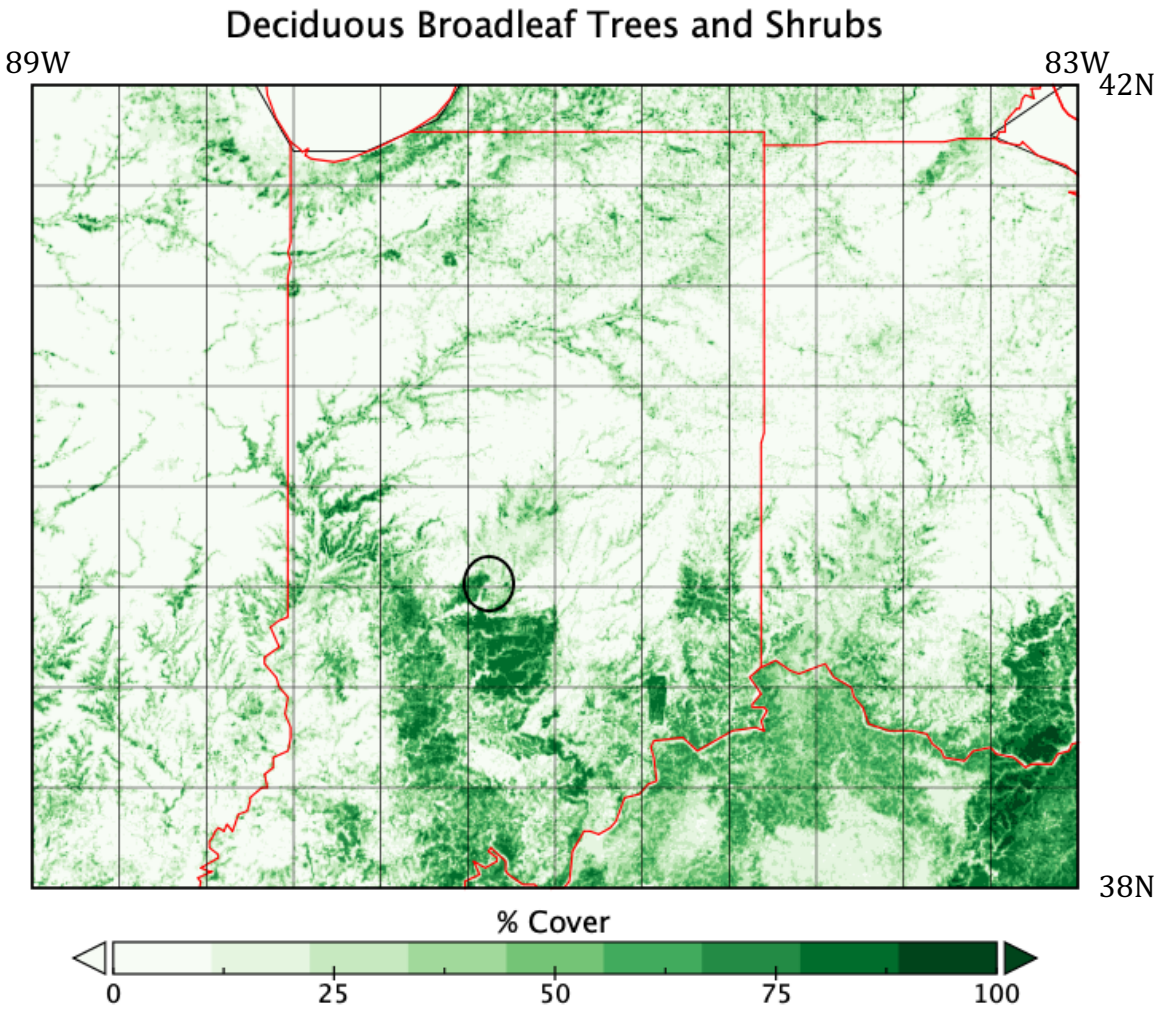

Figure S2: Broadleaf, deciduous trees and shrubs for the region surrounding Beech Island, SC. The black circle denotes the location of Beech Island and its immediate surroundings. The grid is incremented at 0.5° (both latitude and longitude).

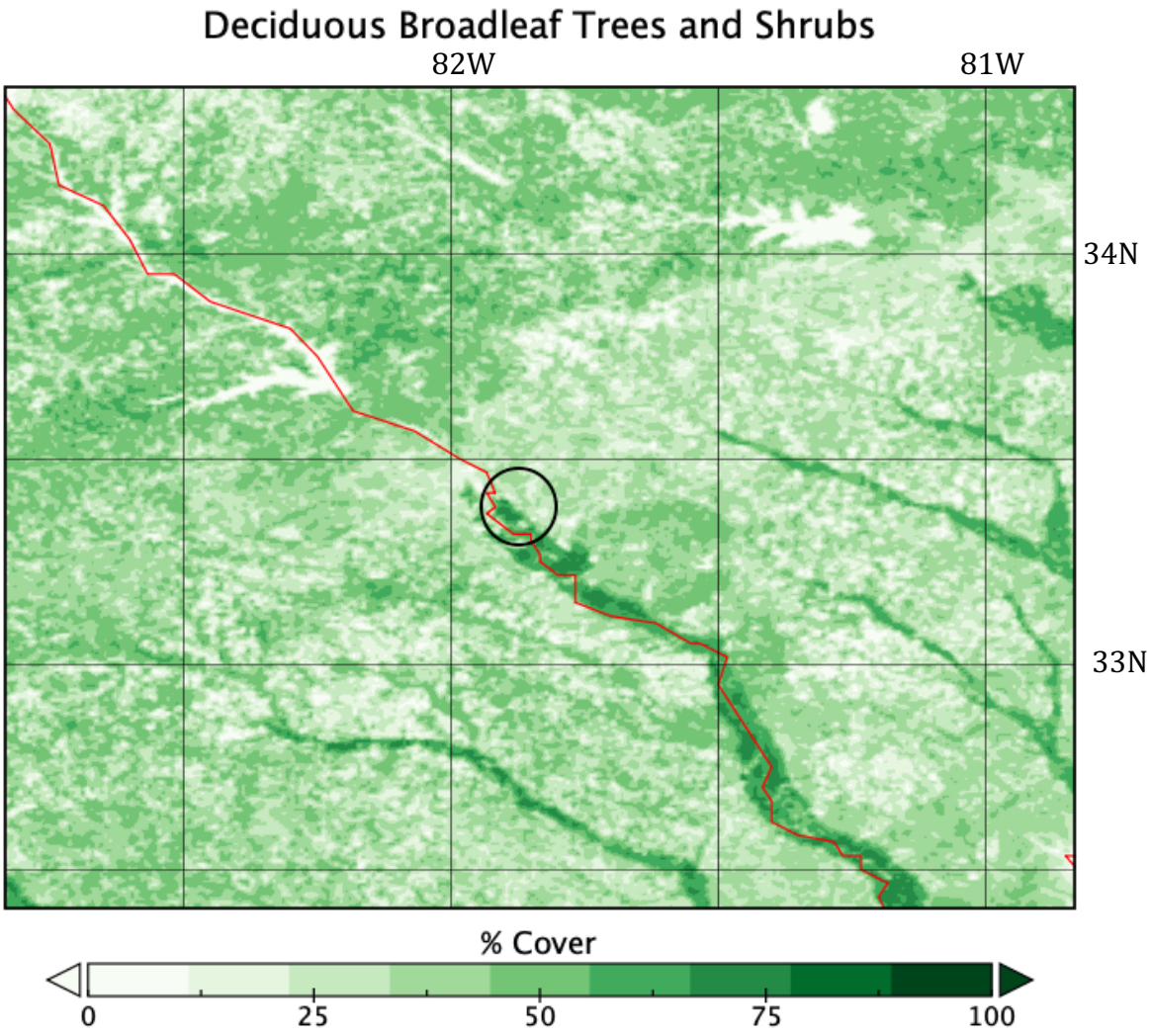

S.2 Simplification of the CO Budget

One of the advantages to the INFLUX experiment is the ability to remove background signals from the urban measurements, and thereby derive the urban enhancement. This approach also allows the CO budget to be simplified. Both the oxidation of CH_4 to CO and the oxidation of CO to CO_2 via the OH radical are reactions that proceed slowly relative to the experimental scale of a few hours transit time. We can consider only this short time scale because we are only considering reactions that can occur when air masses are transiting between the background and urban sites (table S1). Because of this, we calculate that these two processes have negligible impact on our urban CO enhancements, and can be

disregarded given the short reaction time being considered (detailed below, table S1).

The reaction time period can be calculated simply by considering the distance between tower 1 and towers 2 or 3 and the average wind speed. Given the average wind speed during sampling for this study was 4.4 ± 1.3 m s^{-1}, a 2.7-hour transit time is required. In this experiment, we correct our results to account for the incoming background CO and examine the urban contribution alone. This short transit time scale allows us to place constraints on the CH_4 oxidation source and the OH oxidation sink of CO.

Oxidation of CH_4 by OH is a major source of CO globally but CH_4 is long lived in the atmosphere relative to CO (Sander et al., 2006; Atkinson et al., 2006; Duncan et al., 2007). The approximate rate for the reaction of CH4 with OH is 6.4×10^{-15} cm^3 s^{-1} at standard pressure and our mean ambient temperature of 26° C (Atkinson et al., 2006). OH concentration has been determined at urban sites in similar latitude bands and ranges from 1×10^6 cm^{-3} in cool, winter time conditions to 2×10^7 cm^{-3} in hot, summertime conditions (Warneke et al., 2007, 2013; Atkinson and Arey, 2003; Park et al., 2011). We do not have OH concentration measurements at Indianapolis, and therefore use the highest reported literature value for OH of 2×10^7 cm^{-3} (Park et al., 2011) to assess the maximum CH_4 oxidation contribution to CO (Park et al., 2011, Table S1). We calculated the change in mole fraction of CO due to oxidation of CH_4 by OH by:

$$\Delta X_{CO} = \gamma (X_{CH_{4,i}}) \left(1 - e^{-k([OH])t}\right) \qquad (S1)$$

where ΔX_{CO} is the change in CO mole fraction due to CH_4 oxidation by OH, γ is the CO yield for the CH_4+OH reaction (0.96 mole CO produced per mole CH_4), $X_{CH4,i}$ is the initial CH_4 mole fraction (the average CH_4 mole fraction during the sampling period, 1930 nmol:mol), k is the reaction rate for CH_4+OH (6.4×10^{-15} cm^3 s^{-1}), [OH] is the high end member OH concentration from Park et al. (2011) (2×10^7 cm^{-3}, and t is the

transit time of 2.7 hours. Using (S1), we calculated 1.4 nmol:mol CO produced from oxidation of CH_4 between the two towers.

Species	k_{OH} ($cm^3 molec^{-1} sec^{-1}$)	k_{O3} ($cm^3 molec^{-1} sec^{-1}$)	k_{NO3} ($cm^3 molec^{-1} sec^{-1}$)	Estimated Mole Fraction (nmol:mol)	γ_{OH} (%C)	Molec CO per molec VOC	Yield OH (nmol:mol)	Yield O_3 (nmol:mol)	Yield NO_3 (nmol:mol)	Total CO (nmol:mol)	$\Delta\delta^{13}C$ (‰)	$\Delta\delta^{18}O$ (‰)
Methane	6.40E-15		1.00E-18	1930	0.96	0.96	1.4	0	0.005	1.4	-0.21	-0.04
CO	1.44E-13		N/A	166	N/A	N/A	2.4	N/A	N/A	2.4	-0.08	0.17

Table S1: CH_4 and CO deviations caused by oxidation of CH_4 to CO, and oxidation of CO to CO_2 by OH. Assumed [OH] = $2x10^7$ molec cm^{-3} (Park et al., 2011). CO yield from oxidation of CH_4 taken from Grant et al. (2010).

We further assessed the impact on CO isotopes (Table S1) by using the reported isotopic values for CH_4 oxidation (Table 1, main text). We calculated the change in $\delta^{13}C$ and $\delta^{18}O$ by

$$\Delta\delta=\delta_{CO,i}-\frac{(\delta_{CO,i}(X_{CO_i}))+\left(\delta_{CH_4}(X_{CO_{CH_4}})\right)}{\left(X_{CO_i}+X_{CO_{CH_4}}\right)} \qquad (S2)$$

where $\Delta\delta$ is the change in either $\delta^{13}C$ or $\delta^{18}O$, δ_{COi} is the initial delta value at the polluted towers (average of the two towers (non-enhancement) of -29.6‰ for $\delta^{13}C$ and 5.1‰ for $\delta^{18}O$), X_{COi} is the CO mole fraction at the two polluted towers (average value of 166 nmol:mol), δ_{CH4} is the $\delta^{13}C$ or $\delta^{18}O$ value of CO produced by CH_4 oxidation (-52.6‰ and 0‰ for $\delta^{13}C$ and $\delta^{18}O$ respectively, Brenninkmeijer et al., 1999), and X_{COCH4} is the mole fraction of CO produced from oxidation of CH_4 by OH, calculated above.

Using these parameters and the average transit time between the towers of 2.7 hours, we calculate that during the transit across the city, CH_4 oxidation could contribute up to 1.4 nmol:mol CO, changing $\delta^{13}C$ by up to -0.21‰, and $\delta^{18}O$ by up to -0.04‰. These values are below our 1σ measurement uncertainties (0.23‰ $\delta^{13}C$ and 0.46‰ $\delta^{18}O$), and thus we do not consider CH_4 oxidation to be a significant source of CO in our analyses.

OH oxidation is the main sink of CO, and will directly impact the isotopic signatures of CO measured within the city (Röckmann and Brenninkmeijer, 1997; Duncan et al., 2007). Using the same method and OH concentration as for CH_4 oxidation above, and a reaction rate for CO+OH of 1.44×10^{-13} cm^3 s^{-1} (Atkinson et al., 2006), we calculated the loss of CO during the transit of an air mass across the city:

$$\Delta X_{CO} = (X_{CO_i})\left(1 - e^{-k([OH])t}\right) \quad \text{(S3)}$$

We obtained a loss of 2.4 nmol:mol CO. However, to calculate changes to the isotopic budget, we use the fractionation factors for OH oxidation found in Table 1, main text and a Rayleigh distillation approach to compute the impact of the OH sink on $\delta^{13}C$ and $\delta^{18}O$ of CO:

$$\frac{\delta_f}{10^3‰} + 1 = \left(\frac{\delta_i}{10^3‰}\right) f_f^{\alpha-1} + f_f^{\alpha-1} \quad \text{(S4)}$$

f refers to the final change in either $\delta^{13}C$ or $\delta^{18}O$, and i refers to the mean value of $\delta^{13}C$ or $\delta^{18}O$ measured at the two downwind towers (-29.9‰ for $\delta^{13}C$ and 4.1‰ for $\delta^{18}O$). f_f is the final fraction of CO left after the amount of CO lost is removed, determined by:

$$f_f = \frac{X_{CO_T} - X_{CO_{lost}}}{X_{CO_T}} \quad \text{(S5)}$$

where X_{COT} is the total CO mole fraction measured at tower 1 (mean value of 146 nmol:mol), and X_{COlost} is the amount of CO removed by oxidation with OH. α is the fractionation factor for either $\delta^{13}C$ or $\delta^{18}O$ from the literature (Table 1, main text). The estimated total effect of OH oxidation on the CO mole fraction is 2.4 nmol:mol CO lost, -0.08‰ change in $\delta^{13}C$, and 0.17‰ change in $\delta^{18}O$. These changes in the isotopic values can also be neglected in our quantification of the CO isotopic budget given our estimated measurement uncertainty.

Biomass burning can be a source of CO in urban regions, though it is primarily used as a heat source (Saurer et al., 2009). Within Indianapolis, 2/3 of residential and commercial heating is done by natural gas combustion, and the remaining 1/3 is electrical (Gurney et al., 2012). Vimont et al. (2017) estimated that biomass burning for heat was only about 1% of the CO budget during the winter, and did not impact

the isotopic budget significantly. As there should be much less (if any) biomass burning for heat during the summer, we assume that biomass burning is not a significant source of CO. Any biomass burning outside the city (burning off of crop fields or forest fires) is accounted for by removing the background.

The remaining sources of CO that must be considered are oxidation of VOC's (both biogenic and anthropogenic), and fossil fuel combustion. Fossil fuel combustion has long been considered the primary source of CO within urban regions (Stevens et al., 1972; EPA, 2014), whereas only recently has biogenic VOC oxidation been shown to be a significant urban source (Cheng et al., 2017).

S.3 Bootstrap Monte Carlo Results

The bootstrap Monte Carlo method was used to determine the isotopic signatures at Beech Island, South Carolina. A Keeling plot analysis was used to determine these signatures by performing a linear regression on the measured isotopic values plotted against the inverse of the measured mole fraction values. In the bootstrap Monte Carlo, these data were randomly sampled with replacement 1000 times, producing 1000 intercepts from which we took the mean and standard error of the mean as the reported values. To give the reader an idea of the spread in each value, we have included the histograms of the 1000 intercept data sets generated for each isotope in both summer and winter (Figure S1)

Figure S3

(a) Winter $\delta^{13}C$ at Beech Island, South Carolina

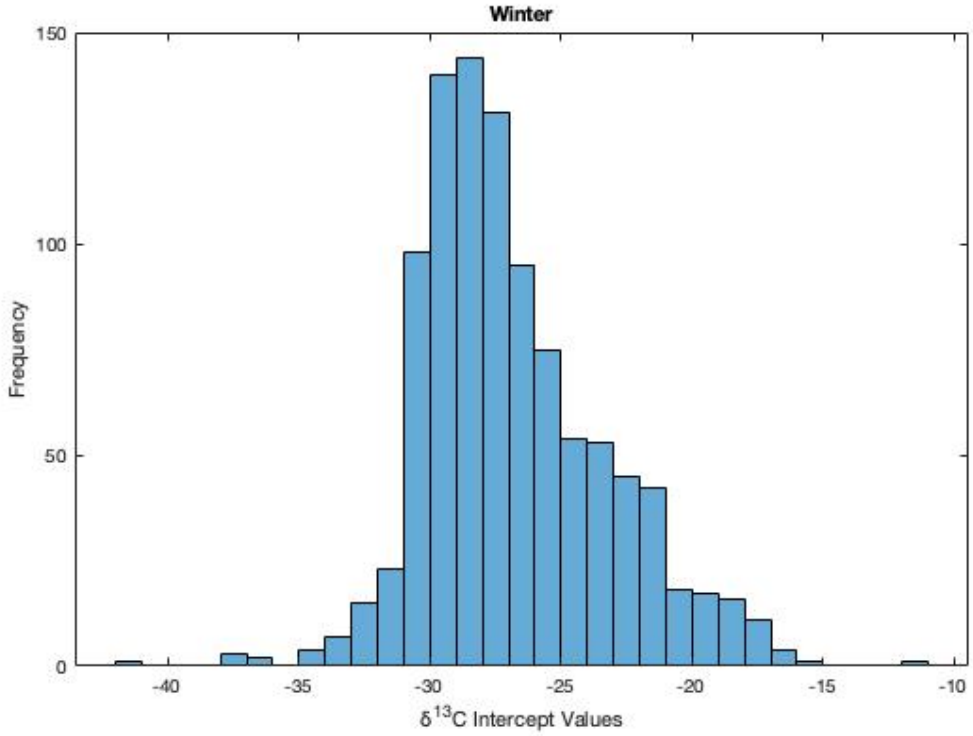

(b) Winter $\delta^{18}O$ at Beech Island, South Carolina

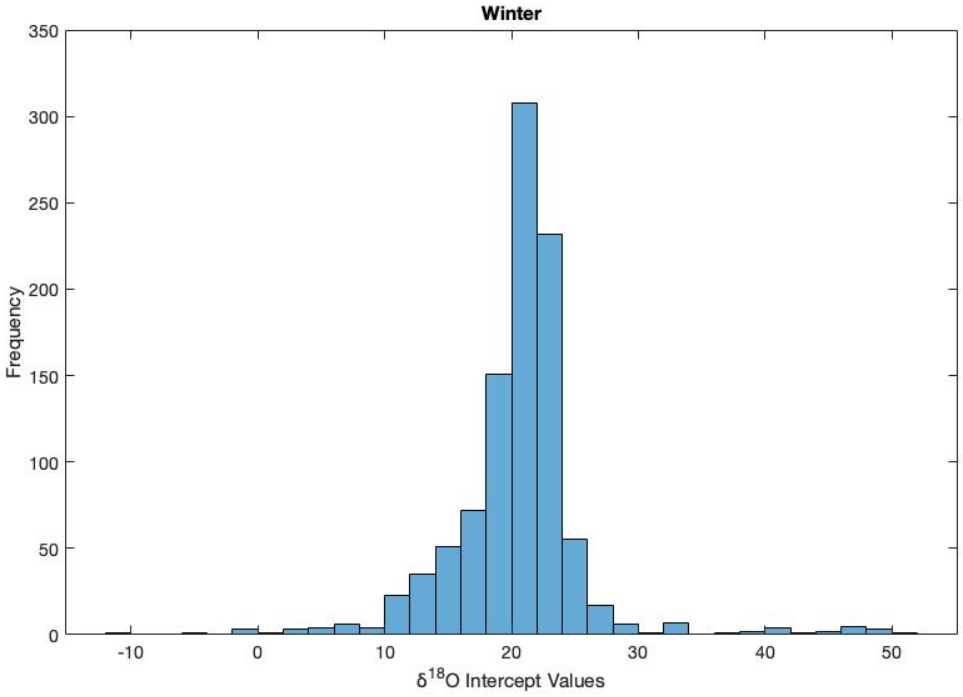

(c) Summer $\delta^{13}C$ at Beech Island, South Carolina

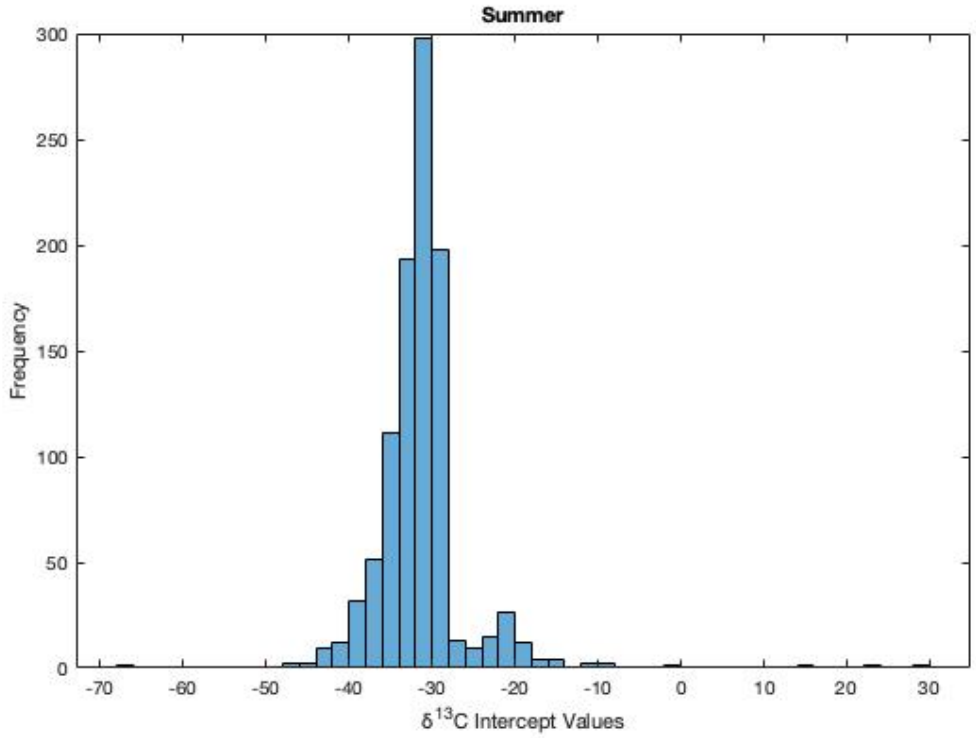

(d) Summer $\delta^{18}O$ at Beech Island, South Carolina

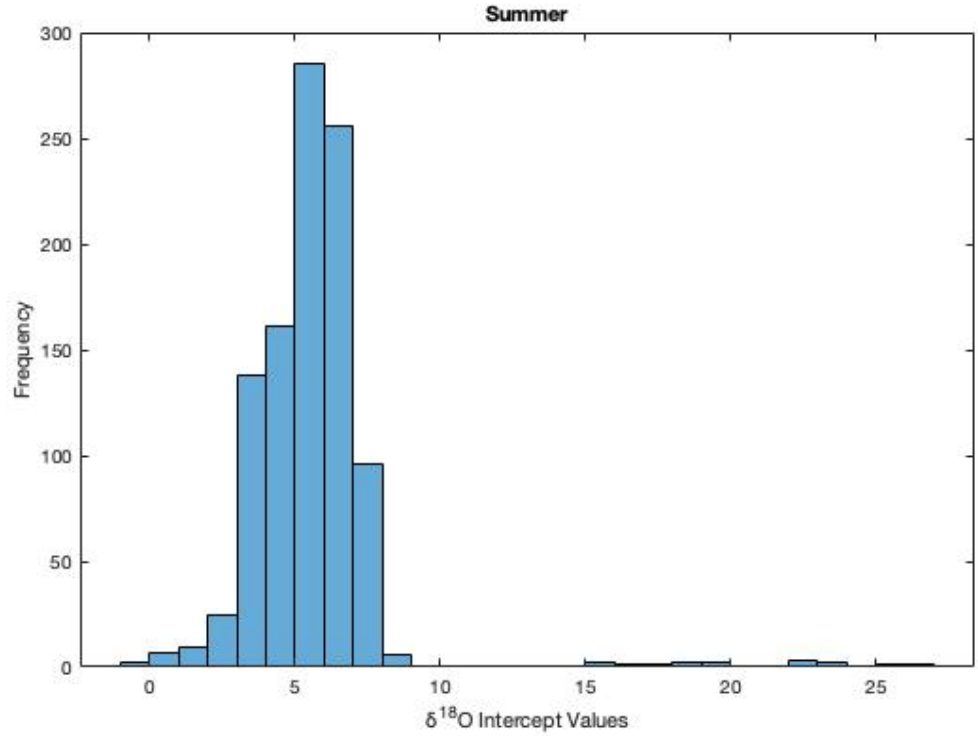

S.4 Mole Fraction and Isotopic Data From Indianapolis, IN, and Beech Island, SC.

Table S2: Indianapolis Tower 1 and Tower 2 mole fraction and isotopic data used in this study. Mole fraction uncertainty is reported as ± 0.5 nmol:mol (1σ).

Date	X_{CO} T1 (nmol:mol)	$\delta^{13}C$ T1 (‰)	1σ $\delta^{13}C$ T1 (‰)	$\delta^{18}O$ T1 (‰)	1σ $\delta^{18}O$ T1 (‰)	X_{CO} T2 (nmol:mol)	$\delta^{13}C$ T2 (‰)	1σ $\delta^{13}C$ T2 (‰)	$\delta^{18}O$ T2 (‰)	1σ $\delta^{18}O$ T2 (‰)
7/27/13	128.2	-29.2	0.04	2.5	0.09	148.1	-29.3	0.04	3.8	0.09
7/29/13	122.9	-28.5	0.04	2.9	0.09	150.4	-30.8	0.04	4.1	0.09
8/1/13	116.6	-28.7	0.04	7.0	0.09	129.0	-29.8	0.04	3.1	0.09
8/2/13	133.9	-30.4	0.04	3.3	0.09	147.9	-30.2	0.04	3.8	0.09
8/7/13	135.2	-32.3	0.04	5.4	0.09	138.1	-32.3	0.04	4.9	0.09
8/27/13	149.6	-31.8	0.04	4.2	0.09	165.7	-32.0	0.04	4.2	0.09
9/10/13	191.1	-31.6	0.13	3.0	0.34	202.7	-32.0	0.13	4.3	0.34
9/11/13	174.6	-31.8	0.13	3.1	0.34	181.6	-31.7	0.13	4.3	0.34
9/18/13	164.2	-29.6	0.13	6.8	0.34	184.2	-30.7	0.13	6.0	0.34
9/19/13	173.3	-30.3	0.13	6.1	0.34	178.5	-30.4	0.13	5.5	0.34
9/20/13	170.5	-29.9	0.13	6.2	0.34	189.1	-29.9	0.13	6.4	0.34
9/29/13	150.8	-28.5	0.13	7.7	0.14	171.3	-29.2	0.13	6.5	0.14
5/12/14	127.2	-28.5	0.18	4.7	0.23	136.7	-28.4	0.18	3.9	0.23
5/16/14	132.4	-26.2	0.18	4.7	0.23	152.7	-26.4	0.18	6.6	0.23
5/17/14	131.5	-25.9	0.18	4.3	0.23	152.3	-26.6	0.18	6.2	0.23
5/27/14	139.6	-29.9	0.18	3.7	0.23	150.0	-29.4	0.18	3.6	0.23
5/28/14	128.9	-29.5	0.18	3.3	0.23	141.4	-29.3	0.18	3.2	0.23
6/3/14	127.8	-28.7	0.18	4.0	0.23	141.0	-27.6	0.18	9.0	0.23
7/29/14	140.2	-29.3	0.20	4.2	0.50	164.0	-29.9	0.20	3.9	0.50
8/12/14	166.6	-29.3	0.29	4.6	0.48	191.5	-29.4	0.29	4.1	0.48
8/13/14	192.3	-29.5	0.29	3.4	0.48	216.1	-29.5	0.29	4.1	0.48
8/19/14	154.4	-31.4	0.29	4.3	0.48	160.5	-30.6	0.29	3.8	0.48
8/20/14	119.5	-30.6	0.29	6.1	0.48	129.2	-30.8	0.29	4.3	0.48
8/21/14	127.4	-33.2	0.29	5.2	0.48	154.5	-31.7	0.29	5.5	0.48
8/22/14	112.4	-31.8	0.29	5.4	0.48	158.6	-31.0	0.29	6.6	0.48
9/1/14	100.3	-31.6	0.15	5.2	0.40	109.5	-32.0	0.15	2.8	0.40
9/2/14	114.1	-30.5	0.15	5.1	0.40	139.7	-30.8	0.15	5.1	0.40
9/3/14	131.1	-30.8	0.15	3.9	0.40	147.6	-30.2	0.15	5.0	0.40
9/5/14	151.3	-31.9	0.15	5.2	0.40	169.0	-31.9	0.15	4.8	0.40
5/5/15	146.9	-28.1	0.31	4.9	0.34	158.0	-28.2	0.31	5.6	0.34
5/15/15	157.3	-29.6	0.31	4.9	0.34	173.4	-29.0	0.31	6.5	0.34
5/22/15	145.1	-26.8	0.31	6.0	0.34	157.5	-26.5	0.31	7.4	0.34
6/5/15	143.8	-29.3	0.31	4.6	0.34	151.3	-28.7	0.31	6.0	0.34
6/8/15	113.9	-30.1	0.31	0.7	0.34	152.7	-28.3	0.31	7.5	0.34
6/30/15	233.1	-29.4	0.25	4.9	0.73	245.8	-29.3	0.25	5.1	0.73
7/6/15	221.6	-30.1	0.25	4.5	0.73	264.3	-29.5	0.25	5.3	0.73
7/14/15	154.7	-30.7	0.25	3.3	0.73	151.3	-30.3	0.25	2.9	0.73
7/17/15	149.2	-34.2	0.25	2.2	0.73	149.6	-32.8	0.25	4.0	0.73
7/25/15	196.6	-30.8	0.25	3.6	0.73	216.1	-29.8	0.25	4.5	0.73
7/29/15	135.3	-33.5	0.25	1.4	0.73	155.7	-32.4	0.25	4.1	0.73

Table S3: Beech Island mole fraction and isotopic data. Mole fraction uncertainty is ± 0.5 nmol:mol (1σ).

Date	X_{CO} (nmol:mol)	$\delta^{13}C$ (‰)	$\delta^{13}C$ 1σ (‰)	$\delta^{18}O$ (‰)	$\delta^{18}O$ 1σ (‰)
4/21/15	152.7	-26.4	0.2	5.7	0.3
5/5/15	152.6	-27.1	0.3	5.4	0.3
5/17/15	124.7	-27.3	0.3	3.5	0.3
6/2/15	109.1	-29.5	0.3	2.0	0.3
6/16/15	142.1	-33.0	0.3	1.1	0.3
7/14/15	143.7	-34.2	0.3	2.7	0.7
7/26/15	179.2	-30.9	0.2	2.4	0.4
8/7/15	157.7	-32.0	0.3	3.3	0.7
8/18/15	87.9	-33.1	0.2	-0.3	0.4
8/28/15	150.8	-30.4	0.2	2.9	0.4
10/6/15	134.0	-29.0	0.2	5.6	0.2
10/20/15	128.5	-28.8	0.2	5.1	0.2
11/3/15	128.1	-29.9	0.2	5.5	0.2
11/17/15	139.3	-28.5	0.2	6.5	0.2
12/9/15	143.7	-28.3	0.2	6.1	0.2
1/2/16	168.5	-27.5	0.2	8.4	0.2
1/12/16	148.0	-27.8	0.2	6.8	0.2
1/27/16	149.0	-27.2	0.2	8.0	0.2
2/10/16	160.6	-27.1	0.2	7.6	0.2
2/24/16	157.3	-27.5	0.2	6.7	0.2
3/9/16	138.4	-26.9	0.2	5.0	0.2

Table S4: Monthly mean CO mole fraction and isotope data extracted from Bräunlich (2000). We were unable to locate a table for these data in the literature, so we used freely available graphical digitizing software (WebPlotDigitizer-4.2, https://automeris.io/WebPlotDigitizer) to extract the data. This software works by selecting points along the axes of a plot, and implements a grid based on the number of pixels between each point. The operator then selects the data from the image, and a table of values is generated by the software. From this data, we took the mean and standard deviation for each month for the sampling period (1996-1999) reported by Bräunlich (2000). We then used the monthly mean values from this data set as a background for the Beech Island Miller Tans analysis.

MONTH	CO	σCO	$\delta^{13}C$	$\sigma\delta^{13}C$	$\delta^{18}O$	$\sigma\delta^{18}O$
1	124.1	14.6	-26.4	0.6	3.5	0.8
2	126.8	17.3	-26.2	0.6	3.5	1.9
3	125.8	18.3	-26.3	0.5	3.3	1.9
4	122.5	20.7	-26.1	0.4	1.8	1.7
5	120.7	15.3	-26.1	0.8	1.5	1.5
6	99.6	14.8	-27.6	0.8	-1.8	1.6
7	85.2	6.6	-29.3	0.7	-3.3	1.3
8	81.6	12.0	-30.1	1.0	-3.0	1.6
9	78.4	11.1	-30.2	1.1	-3.0	1.7
10	91.1	16.4	-28.9	0.9	-1.2	1.4
11	105.5	8.5	-27.9	0.6	1.4	1.6
12	114.6	19.9	-27.2	0.6	2.6	1.6

References

Atkinson, R., and Arey, J.: Gas-phase tropospheric chemistry of biogenic volatile organic compounds: a review, Atmospheric Environment, 37, Supplement 2, 197-219, http://dx.doi.org/10.1016/S1352-2310(03)00391-1, 2003.

Atkinson, R., Baulch, D. L., Cox, R. A., Crowley, J. N., Hampson, R. F., Hynes, R. G., Jenkin, M. E., Rossi, M. J., and Troe, J.: Evaluated kinetic and photochemical data for atmospheric chemistry: Volume II - gas phase reactions of organic species, Atmospheric Chemistry and Physics, 6, 3625-4055, 2006.

Bräunlich, M.: Study of atmospheric carbon monoxide and methane using isotopic analysis, PhD, Institute of Environmental Physics, Rupertus Carola University, Heidelberg, Germany, 2000.

Brenninkmeijer, C. A. M., Rockmann, T., Braunlich, M., Jockel, P., and Bergamaschi, P.: Review of Progress in Isotope Sutdies of Atmospheric Carbon Monoxide, ChemoSphere- Global Change Science, 1, 33-52, 1999.

Cheng, Y., Wang, Y. H., Zhang, Y. Z., Chen, G., Crawford, J. H., Kleb, M. M., Diskin, G. S., and Weinheimer, A. J.: Large biogenic contribution to boundary layer O-3-CO regression slope in summer, Geophysical Research Letters, 44, 7061-7068, 10.1002/2017gl074405, 2017.

Duncan, B. N., Logan, J. A., Bey, I., Megretskaia, I. A., Yantosca, R. M., Novelli, P. C., Jones, N. B., and Rinsland, C. P.: Global budget of CO, 1988–1997: Source estimates and validation with a global model, Journal of Geophysical Research: Atmospheres, 112, D22301, 10.1029/2007jd008459, 2007.

Guenther, A. B., Jiang, X., Heald, C. L., Sakulyanontvittaya, T., Duhl, T., Emmons, L. K., and Wang, X.: The Model of Emissions of Gases and Aerosols from Nature version 2.1 (MEGAN2.1): an extended and updated framework for modeling biogenic emissions, Geosci. Model Dev., 5, 1471-1492, 10.5194/gmd-5-1471-2012, 2012.

Gurney, K. R., Razlivanov, I., Song, Y., Zhou, Y. Y., Benes, B., and Abdul-Massih, M.: Quantification of Fossil Fuel CO2 Emissions on the Building/Street Scale for a Large US City, Environ. Sci. Technol., 46, 12194-12202, 10.1021/es3011282, 2012.

Park, C., Schade, G. W., and Boedeker, I.: Characteristics of the flux of isoprene and its oxidation products in an urban area, J. Geophys. Res.-Atmos., 116, 13, 10.1029/2011jd015856, 2011.

Rockmann, T., and Brenninkmeijer, C. A. M.: CO and CO2 isotopic composition in Spitsbergen during the 1995 ARCTOC campaign, Tellus, 49B, 455-465, 1997.

Röckmann, T., Brenninkmeijer, C. A. M., Saueressig, G., Bergamaschi, P., Crowley, J. N., Fischer, H., and Crutzen, P. J.: Mass-Independent Oxygen Isotope Fractionation in Atmospheric CO as a Result of the Reaction CO+OH, Science, 281, 544-546, 10.1126/science.281.5376.544, 1998.

Sander, S. P., Friedl, R., Golden, D., Kurylo, M., Moortgat, G., Keller-Rudek, H., Wine, P., Ravishankara, A., Kolb, C., and Molina, M.: Chemical kinetics and photochemical data for use in atmospheric studies: evaluation number 15, National Aeronautics and Space Administration, Jet Propulsion Laboratory, California Institute of Technology Pasadena, CA, 2006.

Saurer, M., Prevot, A. S. H., Dommen, J., Sandradewi, J., Baltensperger, U., and Siegwolf, R. T. W.: The influence of traffic and wood combustion on the stable isotopic composition of carbon monoxide, Atmospheric Chemistry and Physics, 9, 3147-3161, 2009.

Stevens, C. M., Kaplan, L., Gorse, R., Durkee, S., Compton, M., Cohen, S., and Bielling, K.: The kinetic isotope effect for carbon and oxygen in the reaction CO + OH, Int. J. Chem. Kinet., 12, 935-948, 10.1002/kin.550121205, 1980.

Stevens, C. M., Krout, L., Walling, D., and Venters, A.: The Isotopic Composition of Atmospheric Carbon Monoxide, Earth and Planetary Science Letters, 16, 147-165, 1972.

Vimont, I. J., Turnbull, J. C., Petrenko, V. V., Place, P. F., Karion, A., Miles, N. L., Richardson, S. J., Gurney, K. R., Patarasuk, R., Sweeney, C., Vaughn, B., and White, J. W. C.: Carbon monoxide isotopic measurements in Indianapolis constrain urban source isotopic signatures and support mobile fossil fuel emissions as the dominant wintertime CO source, Elem Sci Anth, 5, 10.1525/elementa.136, 2017.

Warneke, C., de Gouw, J. A., Edwards, P. M., Holloway, J. S., Gilman, J. B., Kuster, W. C., Graus, M., Atlas, E., Blake, D., Gentner, D. R., Goldstein, A. H., Harley, R. A., Alvarez, S., Rappenglueck, B., Trainer, M., and Parrish, D. D.: Photochemical aging of volatile organic compounds in the Los Angeles basin: Weekday-weekend effect, J. Geophys. Res.-Atmos., 118, 5018-5028, 10.1002/jgrd.50423, 2013.

Warneke, C., McKeen, S. A., de Gouw, J. A., Goldan, P. D., Kuster, W. C., Holloway, J. S., Williams, E. J., Lerner, B. M., Parrish, D. D., Trainer, M., Fehsenfeld, F. C., Kato, S., Atlas, E. L., Baker, A., and Blake, D. R.: Determination of urban volatile organic compound emission ratios and comparison with an emissions database, J. Geophys. Res.-Atmos., 112, 13, 10.1029/2006jd007930, 2007.